Semimetallicity of free-standing hydrogenated monolayer boron from MgB_2

I. Tateishi,[1] N. T. Cuong,[2,3] C. A. S. Moura,[4,5] M. Cameau,[6,5] R. Ishibiki,[3] A. Fujino,[3] S. Okada,[3] A. Yamamoto,[7,8] M. Araki,[5] S. Ito,[5] S. Yamamoto,[5] M. Niibe,[9] T. Tokushima,[9] D. E. Weibel,[4] T. Kondo,[3,8] M. Ogata,[1] and I. Matsuda[5,*]

[1]*Department of Physics, School of Science, University of Tokyo, Hongo, Tokyo 113-0033, Japan*
[2]*International Center for Young Scientists, National Institute for Materials Science, Tsukuba, 305-0044, Japan*
[3]*Graduate School of Pure and Applied Sciences, University of Tsukuba, Tsukuba, 305-8571, Japan*
[4]*Institute of Chemistry, UFRGS, Porto Alegre, Rio Grande do Sul, Brazil*
[5]*Institute for Solid State Physics, University of Tokyo, Kashiwa, Chiba, 277-8581, Japan*
[6]*Institut des Nanosciences de Paris, Sorbonne Universite, Paris, 75005, France*
[7]*Institute of Engineering, Tokyo University of Agriculture and Technology, Tokyo, 183-8538, Japan*
[8]*Materials Research Center for Element Strategy, Tokyo Institute of Technology, Yokohama, 226-8503, Japan*
[9]*Laboratory of Advanced Science and Technology for Industry, University of Hyogo, Hyogo, 678-1205, Japan*

(Received 10 December 2018; revised manuscript received 20 January 2019; published 22 February 2019)

Electronic states of a free-standing hydrogenated monolayer boron (HB) sheet were studied via soft x-ray spectroscopies at the B K-shell absorption edge and first-principles calculations. The HB sheet is semimetallic with electron and hole pockets at the Y and Γ points, respectively. The electron band results from the B-H-B bonds formed during synthesis from a MgB_2 crystal, while the hole band is kept through the process and originates from a honeycomb lattice boron layer or borophene in MgB_2. Our results suggest that the HB sheet is a promising two-dimensional material for realizing new boron-based or superconducting nanodevices.

DOI: 10.1103/PhysRevMaterials.3.024004

I. INTRODUCTION

Two-dimensional (2D) monatomic layers in van der Waals crystals or on solid surfaces have wide attention because of their unique physical properties and potential applications in quantum devices [1–5]. Specifically, there is growing interest in layers of Xenes such as silicene [6–9], germanene [10–12], and bismuthene [13] that show nontrivial topological phases. Recently, borophene layers were discovered and found to have Dirac fermions [14–18]. These Xenes show that such layers can go beyond graphene and can be used to explore exotic properties and design new quantum nanoscale devices. However, in contrast to graphene, these Xene layers form only on solid surfaces, significantly limiting their applications. It is thus necessary to develop technology to peel the layer from the surface and passivate it chemically so it can be placed on any substrate under ambient conditions [19].

A different approach is to prepare a free-standing hydrogen boride (HB) sheet that corresponds to hydrogenated monolayer boron or borophane. The atomic sheet is synthesized from a MgB_2 crystal by using a proton ion-exchange reaction and liquid exfoliation [20]. In this work, we investigate the electronic structure of the HB sheet via soft x-ray absorption and emission spectroscopy (XAS and XES) at the B K-shell absorption edge. We also carry out first-principles calculations to explore their detailed band dispersion curves. The HB sheet is semimetallic with an electron pocket at the Y point and a hole pocket at the Γ point in the two-dimensional (2D) Brillouin zone. The electron band results from hydrogenation of the borophene layer. However, the hole band is kept from a boron layer of the honeycomb lattice or borophene in a MgB_2 crystal, carrying over properties of the mother material.

II. EXPERIMENTS AND CALCULATIONS

Formation of HB sheets with a B : H ratio of 1 : 1 proceeds through the proton ion-exchange reaction of magnesium diboride (MgB_2): $MgB_2 + 2H^+ \rightarrow Mg^{2+} + 2HB$. Figure 1(a) schematically shows the synthesis, which consists of adding MgB_2 powder to a methanol solution with an ion-exchange resin and exfoliating in the solution. The process was done at room temperature under a nitrogen atmosphere. The supernatant liquid contained the HB sheets, which were collected after drying [Fig. 1(b)]. The sheets of the free-standing HB were confirmed by scanning electron microscopy [see Fig. 1(c)]. Synthesis of the HB layers consisted of peeling honeycomb boron layers in a MgB_2 crystal with hydrogen termination (borophane). Thus the HB sheets in Fig. 1(c) correspond to layers in Fig. 3(a) that consist of a hydrogen and a single boron layer, and originate from MgB_2. More detail on the synthesis and characterization of hydrogen boride sheets or borophane layers can be found elsewhere [20].

Sample characterizations, including B K-edge XES and XAS, were made at the beamline BL-09A of the New-SUBARU Synchrotron Radiation Facility at the University of Hyogo [21–24] and SPring-8 BL07LSU [25]. All first-principles calculations were performed using density functional theory (DFT) [26,27] as implemented in Quantum ESPRESSO [28].

*imatsuda@issp.u-tokyo.ac.jp

 ©2019 American Physical Society

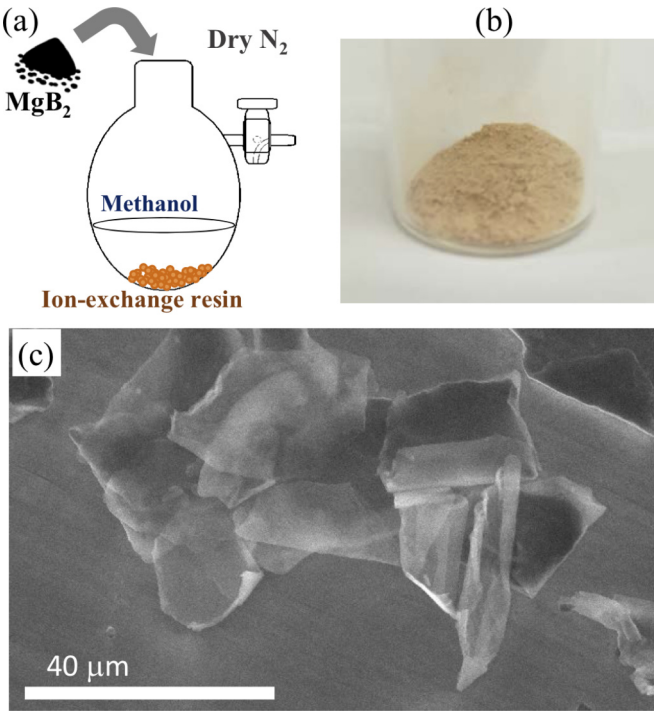

FIG. 1. (a) Schematic of the preparation procedure, (b) photograph of the sample powder, and (c) scanning electron microscope image of the free-standing hydrogen boride (HB) samples.

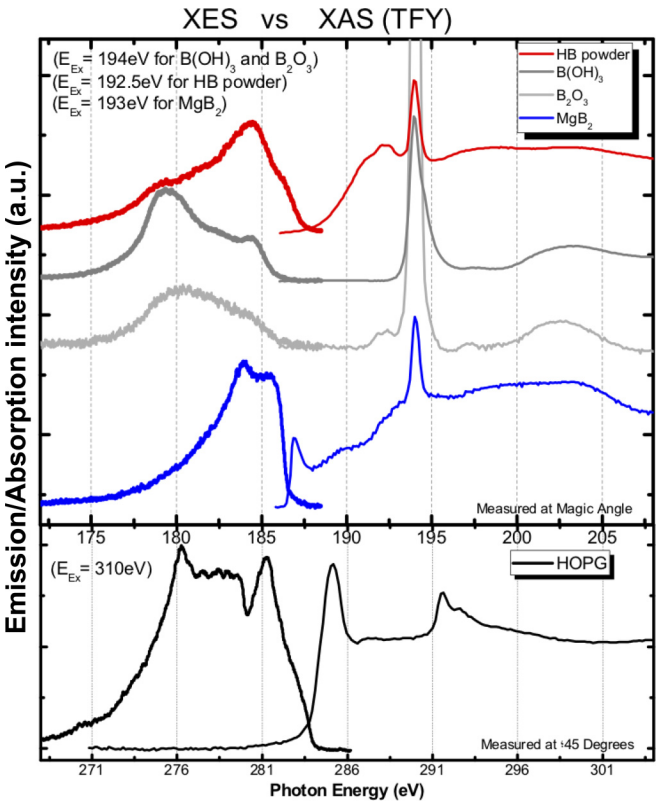

FIG. 2. B *K*-edge XES and XAS spectra of powder samples of HB sheets (borophane), $B(OH)_3$, B_2O_3, and MgB_2. C *K*-edge XES and XAS spectra of the highly oriented pyrolytic graphite (HOPG) sample are shown for comparison. The excitation energy (E_{EX}) from XES measurements of the samples is shown in the figure. The elastic scattering Rayleigh peaks in the XES spectra are removed to show the fine spectral features. The incident angle was set at 35° from the surface normal (magic angle) [30] or at 45°.

III. RESULTS AND DISCUSSIONS

A. X-ray absorption and emission spectroscopy

To examine occupied and unoccupied electronic states of the HB sheets, Fig. 2 shows a collection of B *K*-edge XAS and XES data of powder samples of HB sheets (borophane), $B(OH)_3$, B_2O_3, and MgB_2. Spectra of near-edge x-ray absorption fine structure were recorded with total fluorescence yield and analyzed with the software package ATHENA [29]. We used commercial powders of $B(OH)_3$(99.5%, Wako Pure Chemical Industries, Osaka, Japan), B_2O_3 (Kanto Chemical Co., Tokyo, Japan), and MgB_2 (99%, Rare Metallic Co., Tokyo, Japan).

The C *K*-edge XAS and XES spectra of the highly oriented pyrolytic graphite (HOPG) crystal are also shown for comparison. The insulating samples of $B(OH)_3$ and B_2O_3 show energy gaps, whereas spectra of HB and MgB_2 overlap each other in XAS and XES [31,32]. The appearance is the same as that of HOPG, which is the standard reference for a gapless material [21]. Figure 2 is direct evidence that the HB sheet and MgB_2 crystal have a gapless electronic structure at the Fermi level. We note that an XES peak at 194 eV is assigned to B–O bonds, showing that these HB and MgB_2 samples may have been contaminated by oxygen atoms, most likely during the sample transfer before the spectroscopic measurements. Thus the result is a sum of clean and oxide regions in the HB sheet and MgB_2 crystal. However, there are no band gaps in either sample. Therefore, one observes only the signals from the gapless electronic states.

We note here that the HB sheet is now only synthesized as a powder or a random assembly of the monoatomic layers. We leave more accurate mapping of structural topography or electronic state by scanning tunneling microscope or angle-resolved photoemission spectroscopy for the future measurements of a flat HB sheet with wide-area and the well-defined orientation. On the other hand, the averaged microscopic data are identical to the macroscopic x-ray absorption/emission spectra. Thus, the present data of x-ray spectroscopies are sufficient to make comparisons to the theoretical calculation.

B. DFT results: Evolution of band dispersion curves

After the chemical treatments in Fig. 1, the honeycomb boron layer terminates with hydrogen atoms, forming a sheet of hydrogen boride (borophane), as shown in Fig. 3(a). The atomic structure is directly derived as a local structure based on the combination of an x-ray pair distribution function with DFT calculations, and further confirmed by x-ray photoelectron spectroscopy, ultraviolet absorption spectroscopy, and Fourier-transformed infrared reflection spectroscopy [20]. The bond configuration in the sheet is similar to that of diborane, which forms a two-electron three-atom bond structure in B–H–B [33–36]. Here we note that the hexagonal structure of HB sheet is slightly distorted, compared to the

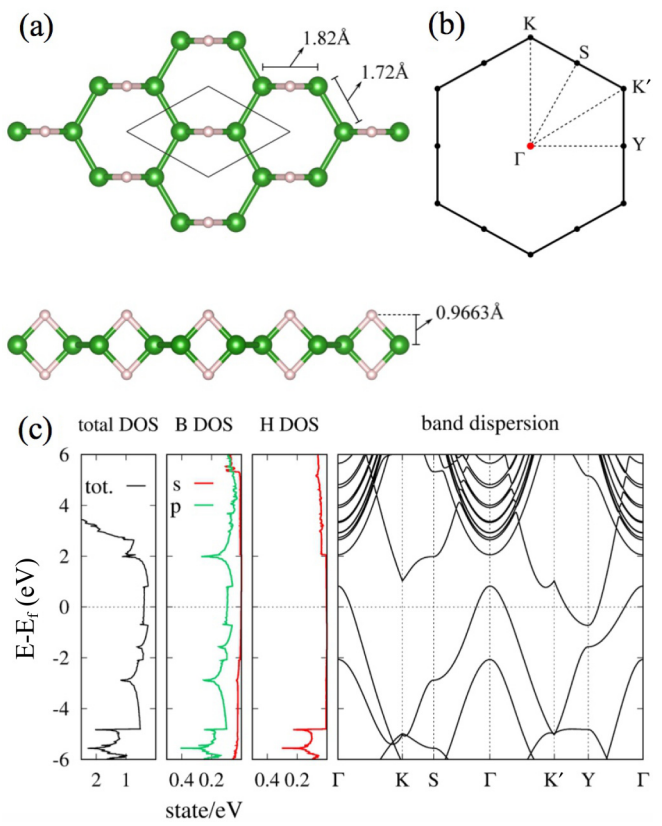

FIG. 3. (a) Atomic structure of the HB layer (borophane), (b) two-dimensional Brillouin zone, and (c) calculated density of states (DOS) and band dispersion curves along the k-path in the Brillouin zone. In the partial DOS panel, DOS is projected into components of angular momentum. Red line and green line show s-orbital and p-orbital, respectively. In (a), boron and hydrogen atoms are shown as green and white balls, respectively. Bond drawings are defined by interatomic distance.

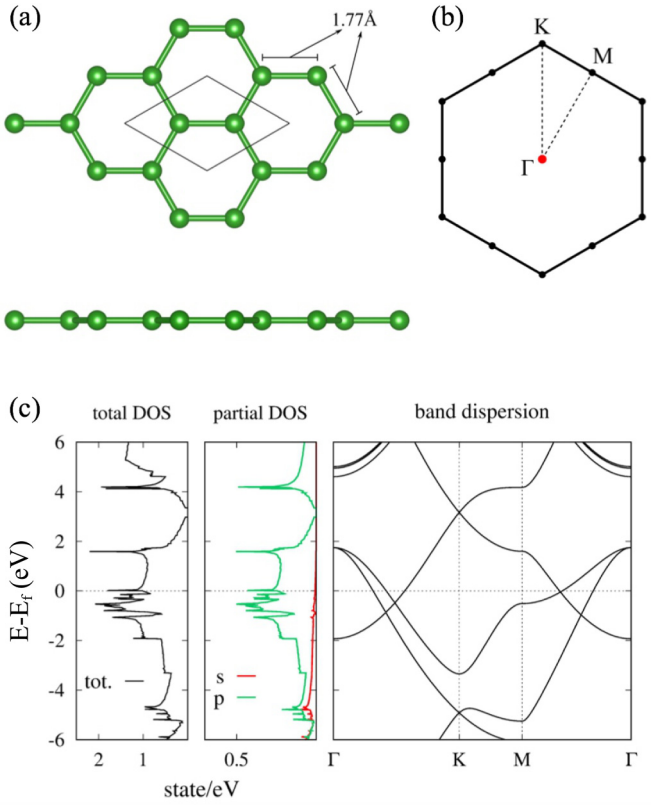

FIG. 4. (a) Atomic structure of a boron layer of the honeycomb lattice (borophene), (b) two-dimensional Brillouin zone, and (c) calculated DOS and band dispersion curves along the symmetry axes in the Brillouin zone. In (a), boron atoms are shown as green balls. Bond drawings are defined by interatomic distance.

hexagonal honeycomb boron layers in MgB_2 crystal due to the hydrogenation.

On the basis of the atomic model in Fig. 3(a), the electronic band structure is calculated along symmetric axes in the 2D Brillouin zone after the optimization of structure [Fig. 3(b)]. Our DFT calculations [26–28] used the generalized gradient approximation (GGA) with nonrelativistic Perdew-Burke-Ernzerhof parametrization [37] for the exchange correlation term. The Kohn-Sham orbitals were expanded by using a plane-wave basis with cutoff energies of 50 and 250 Ry. The Brillouin zone was sampled on a $32 \times 32 \times 1$ k-point grid.

The band dispersion in Fig. 3(c) shows that the HB sheet is semimetallic with an electron pocket around the Y point and a hole pocket around the Γ point. The calculated electronic state has Fermi surfaces and finite density of states (DOS) at the Fermi level (E_f), thus, consistent with the experimental spectra in Fig. 2. For comparison, the electronic band structure of a honeycomb boron layer, or borophene, was calculated as shown in Fig. 4. The band structure is metallic with two hole pockets and one electron pocket around the Γ point, making loops of Dirac nodal lines (DNLs).

Comparing electronic structures of the HB sheet and borophene shows drastic change. Hydrogenation or adsorption of the heteroatoms has a significant effect on an original layer and often induces new functions [38,39]. Here evolution of the electronic states is tracked through formation of the B-H-B bonds. Figure 5 shows the electronic band structures of hypothetical materials of hydrogen boride whose hydrogen atoms are placed symmetrically at $7.50c$ from the boron layer, $5.00c$, $4.00c$, and so on, down to c, here $c = 0.9663$ Å is the optimized result of HB sheet. The band dispersion of the material with hydrogen atoms at 7.50 c is composed of electronic states of pristine borophene and hydrogen atoms near the Fermi level. Because hydrogen atoms are almost isolated from the boron layer, two bands originated from H atoms are nearly degenerated (A_g and B_{1u}). These two bands cross other bands originating from the boron layer and have dispersion that comes from H-H hopping terms. As the H atoms approach the boron layer, the dispersion curves change with energy shifts. In particular, energy of the electron-like B_{1u} band at the Γ point increases and, when the hydrogen atoms are below $2.00c$, it goes above the A_g band leading to the disappearance of DNL. However, the B_{1g} band at the Γ point forming a hole pocket remains unchanged by the decrease of the hight of hydrogen atoms. On the other hand, at the Y point, a B_{2g} band decreases. Consequently, when the hydrogen atoms are at c, i.e., for the case of the HB sheet, there are only two bands at the Fermi level: One is an electron pocket at the Y point, formed by the B-H-B bonds, and the

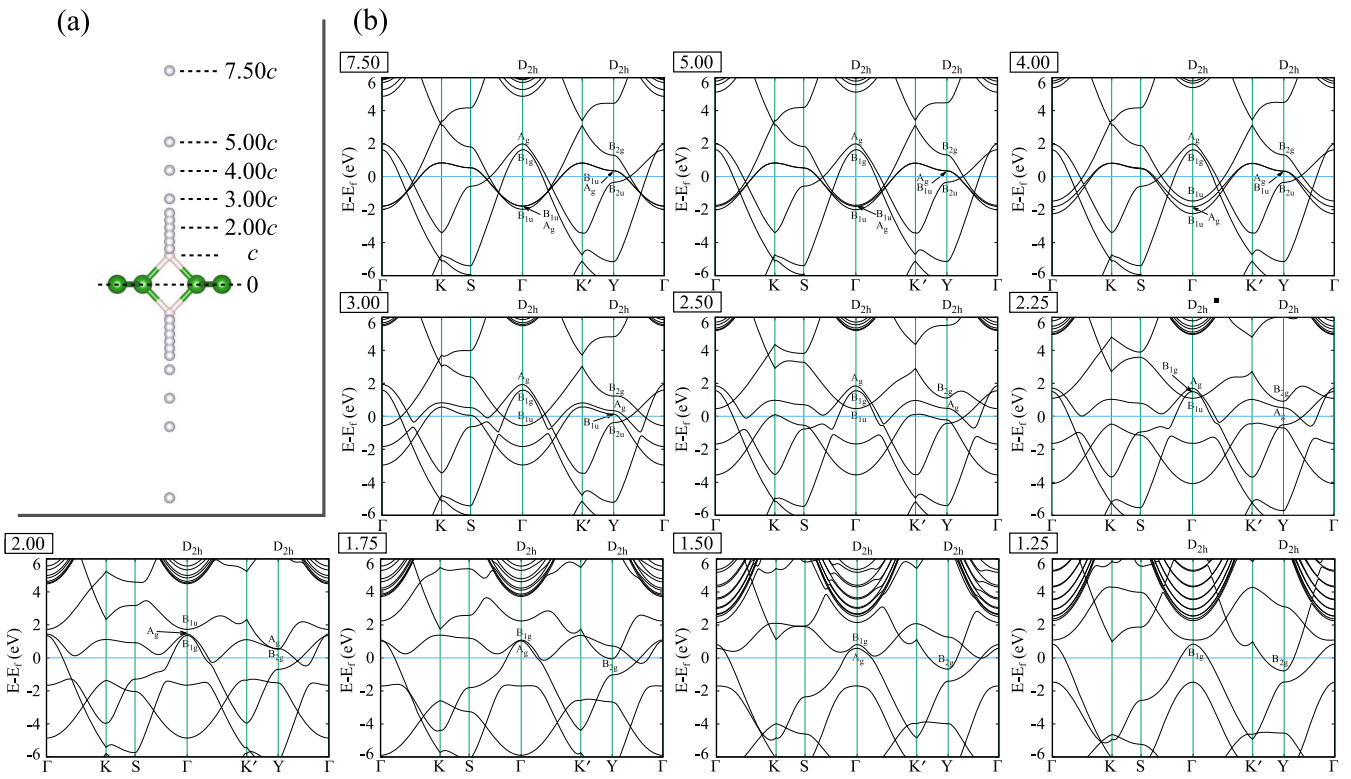

FIG. 5. Evolution of band structure from borophene to the HB sheet, tracked by changing hydrogen height. Here, hydrogen height is written with the unit of $c = 0.9663$ Å, which is the optimized result of the HB sheet. (a) A schematic picture of hydrogen height. Green balls represents boron atoms, white and gray balls represents hydrogen atoms. Two hydrogen atoms located at c are shown as white balls. (b) The electronic band structure for each hydrogen height. The hydrogen height is shown at top left of each panel. On Γ point and Y point, the bands around the Fermi level are labeled by the corresponding irreducible representations.

other is a hole pocket at the Γ point, which remains from borophene.

C. DFT results: Spatial distributions of the 2D electronic states

To clarify the electronic nature in the HB sheet, further calculations were made to draw the spatial distributions of the wave function, compared to the electronic states of MgB_2 that has a borophene layer in the crystal. In the first-principles total-energy calculations, ultrasoft pseudopotentials were used to describe the electron-ion interaction [40]. Valence wave functions and augmented charge density were expanded using plane-wave basis sets with cutoff energies of 60 and 480 Ry, respectively. Both the internal atomic coordinates and lattice parameters of the MgB_2 crystal and monolayer HB were optimized until the residual forces acting on each atom were less than 10^{-4} Ry/Bohr. The atomic geometry of the honeycomb boron monolayer was used as the boron sheet for the optimized MgB_2 crystal. We used $1 \times 1 \times 1$ and 1×1 unit cells for the MgB_2 crystal and HB (or boron) monolayer, respectively. To simulate the isolated boron and HB monolayers, the sheet was separated by periodic images with a vacuum region of 15 Å.

Figure 6 shows the calculated electronic structure of MgB_2 crystal. The crystal structure of MgB_2 is composed of single layers of a honeycomb boron lattice (borophene) with magnesium ions, as shown in Fig. 6(a). The band structure of the MgB_2 crystal shows that the crossing bands at the Fermi level originate from boron orbitals [Fig. 6(b)]. The wave function distribution of the δ_1, δ_2, and δ_3 bands at the Γ point shown in Fig. 6(c) supports this picture. This is consistent with previous findings that electronic properties, such as superconductivity, are determined by the boron layers [41–43]. Along the in-plane directions (Γ-M or Γ-K), there are two hole pockets (labeled δ_1 and δ_2) and one electron pocket (labeled δ_3) at the Γ point. The two dispersions corresponding to δ_1 and δ_2 cross the dispersion of δ_3 at about -2 eV below the Fermi level and form the Dirac points. As we can see from Fig. 6(c), these two hole pockets are derived from the boron p_x, p_y, and s orbitals (i.e., σ-bonds), while the electron pocket is from the boron p_z orbital. The wave functions of the former are symmetric with respect to the boron plane and the wave function of the latter is asymmetric. The color of the wave function distrubution in Fig. 6(c) corresponds to the sign of wave function and it supports this picture. This opposite symmetry restricts the hybridization between them and, consequently, the bands cross each other resulting in the DNLs around the Γ point in MgB_2.

Here it is to be noted that the energy-band structure near Fermi energy in Fig. 6(b) for MgB_2 coincides quite well with the band structure for the borophene shown in Fig. 4(c). However, the entire band energy in Fig. 6(b) is about 2 eV lower than that in Fig. 4(c) because of electron doping from Mg atoms to the boron layer in the case of MgB_2. Here the

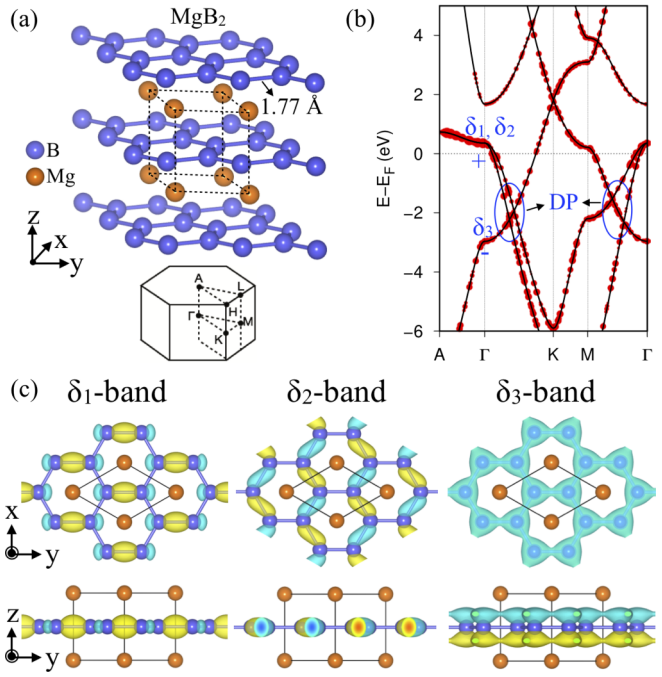

FIG. 6. (a) Atomic structure and the Brillouin zone, (b) calculated energy-band structure of a MgB_2 crystal, and (c) wave function distribution of the δ_1, δ_2, and δ_3 bands of MgB_2 at the Γ point. In (a), boron and magnesium atoms are shown as blue and orange balls, respectively, while the unit cell is shown by the dashed line. In (b), the red dots are the projected band structure of MgB_2 on B atoms, and E_F is the Fermi energy. "DP" means Dirac point. Dirac points shown in (b) are "cross sections" of DNL. In (c), the color of wave functions corresponds to the sign of wave functions.

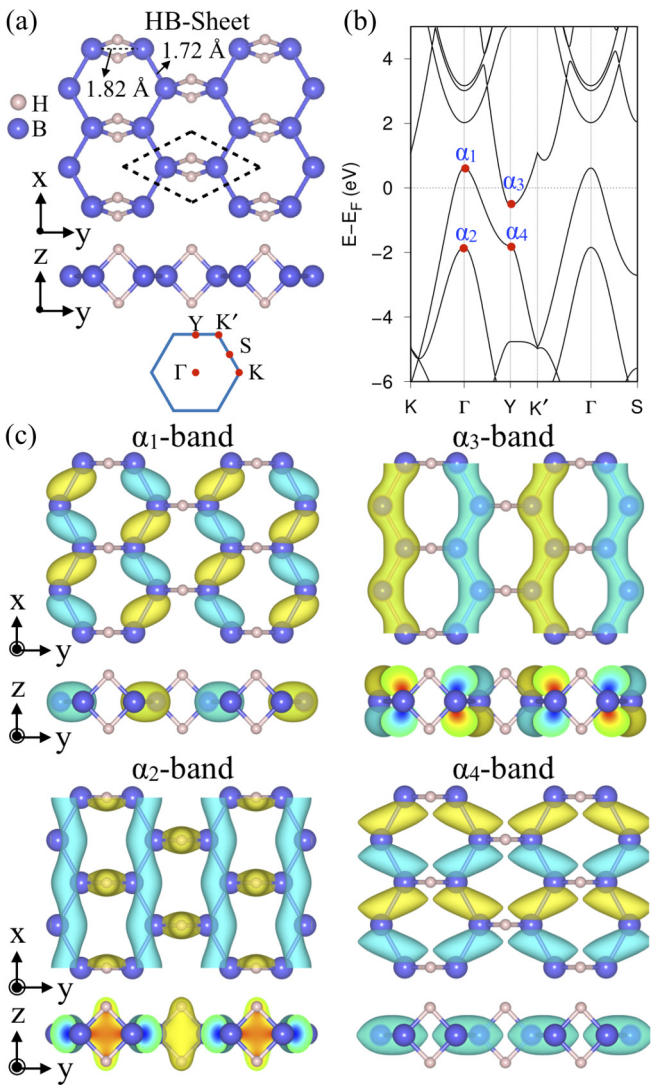

FIG. 7. (a) Atomic structure, (b) Brillouin zone and calculated energy-band structure of a hydrogen boride (HB) monolayer, and (c) wave function distribution of the α_1, α_2, α_3, and α_4 bands of the HB sheet at the Γ and Y points. In (a), boron and hydrogen atoms are shown as blue and white balls, respectively, while the unit cell is shown by the dashed line. Bond drawings are defined by interatomic distance. In (c), the color of wave functions corresponds to the sign of the periodic part of Bloch wave functions.

band originated from the Mg cation does not appear around Fermi energy. These comparisons show that the DNL is the main characteristic of the boron layer and is protected owing to the parity of the mirror symmetry of the atomic sheet.

To compare to the electronic states in the boron layer, the wave function distribution of the HB bands, α_{1-4}, is plotted in Fig. 7. The color of the wave function distribution corresponds to the sign of the wave function. Here, in space group #65, the Y point is one of the time-reversal invariant momenta. Thus, under time-reversal symmetry, the periodic part of the Bloch wave function on the Y point can be written by a real function and the sign of the wave function is well defined [44]. As discussed in Fig. 5, the B_{1g} band at the Γ point remains unchanged by the decrease of the height of hydrogen atoms, which corresponds to the α_1-band in Fig. 7. This picture is supported by the spatial distribution of the α_1-band because it is the same as that of the δ_2 band in Fig. 6(c). The α_4-band at the Y point also has a similar wave function distribution since it is connected to the α_1-band.

On the other hand, the α_3-band, an electron pocket at the Y point, has an out-of-plane distribution of anisotropic electronic states along boron atoms, as shown in Fig. 7. For the α_2-band at the Γ point, electrons are distributed between hydrogen and boron atoms, visualizing the B-H-B bonding state. These calculations show the anisotropic electronic nature of the semimetallic HB sheet. In particular, it is important that the wave function of the hole-like α_1-band is symmetric with respect to the boron plane, while that of the electron-like α_3-band is asymmetric, indicating that these bands will not have hopping integrals between them.

An intriguing result of the calculation is the conservation of the electronic characteristics of the boron sheet in a MgB_2 crystal even after hydrogenation, although the DNL disappears. Since electronic states in the boron layer in MgB_2 are responsible for the superconducting transition at 39 K [41–43], our research shows a possibility that the HB sheet or a derivative may become a superconductor and, therefore, could be a new 2D material for superconductive nanodevices. We note that the borophene layer is theoretically predicted to be superconducting below 10 K [45,46].

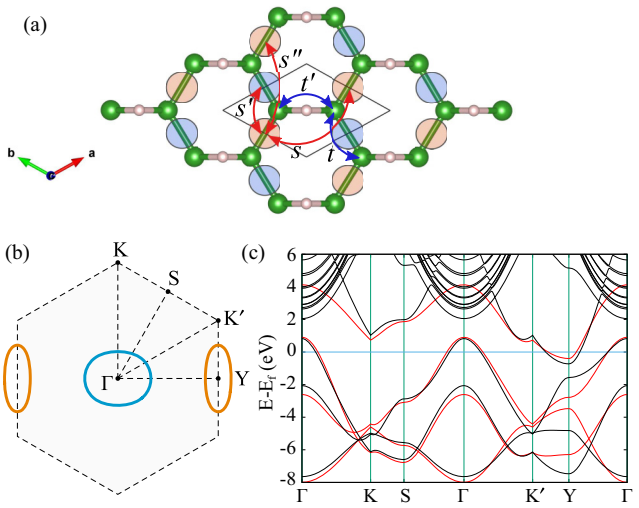

FIG. 8. (a) The hoppings considered in the tight-binding model, (b) Fermi surface, and (c) electronic band structure gained from the model. In (a), boron atoms are shown as green balls and hydrogen atoms are shown as white balls. Red circles and blue circles represent the bases used to describe the hole-pocket. The hoppings used in electron-pocket part are shown with blue arrows and that used in hole-pocket part are shown with red arrows. In (b), the Fermi surface of hole-like band is shown as blue line and that of electron-like is shown as yellow line. In (c), the electronic band structure of DFT result (black lines) and tight-binding model (red lines) are compared.

D. Tight-binding model for the electron- and hole-pocket in HB sheet

As explained in the preceding section, the hole-like band and the electron-like band have opposite parity of the mirror symmetry and hopping integral between them must vanish. Thus tight-binding models for the electron and hole pocket can be constructed independently. Now we assume the boron atoms make a honeycomb lattice, while the optimized HB sheet has a deformed honeycomb structure. We also neglect the spin degree of freedom.

The electron-like α_3-band on the Y point consists of the p_z-orbital of boron atoms. The tight-binding model should be

$$\begin{aligned} H = &-t\sum_j \left(c^\dagger_{\mathrm{A},\boldsymbol{R}_j} c_{\mathrm{B},\boldsymbol{R}_j+\boldsymbol{a}_1} + c^\dagger_{\mathrm{A},\boldsymbol{R}_j} c_{\mathrm{B},\boldsymbol{R}_j-\boldsymbol{a}_2}\right) + \mathrm{H.c.} \\ &-t'\sum_j \left(c^\dagger_{\mathrm{A},\boldsymbol{R}_j} c_{\mathrm{B},\boldsymbol{R}_j} + \mathrm{H.c.}\right) \\ &+\mu_e \sum_j \left(c^\dagger_{\mathrm{A},\boldsymbol{R}_j} c_{\mathrm{A},\boldsymbol{R}_j} + c^\dagger_{\mathrm{B},\boldsymbol{R}_j} c_{\mathrm{B},\boldsymbol{R}_j}\right), \end{aligned} \tag{1}$$

where $c_{\mathrm{A},\boldsymbol{R}_j}$ and $c_{\mathrm{B},\boldsymbol{R}_j}$ ($c^\dagger_{\mathrm{A},\boldsymbol{R}_j}$ and $c^\dagger_{\mathrm{B},\boldsymbol{R}_j}$) are the annihilation (creation) operators of the electron on the A sublattice and B sublattice in the unit cell whose origin is located at $\boldsymbol{R}_j$. $\boldsymbol{a}_1$ and $\boldsymbol{a}_2$ are the basis vector of the honeycomb lattice: $\boldsymbol{a}_1 = (\frac{\sqrt{3}}{2}a, \frac{1}{2}a)$ and $\boldsymbol{a}_2 = (-\frac{\sqrt{3}}{2}a, \frac{1}{2}a)$, with a being the lattice constant. Here we assumed only the nearest-neighbor hoppings [Fig. 8(a)]. The x-direction hopping, t', will be larger than t since there are additional electron hopping path through the hydrogen atoms in between. μ_e in the last term represents the one-body energy level. Actually, the parameters are estimated by using Wannier90 [47], $t = 1.13$ eV, $t' = 3.80$ eV, $\mu_e = -1.935$ eV.

The energy dispersion is given by

$$\begin{aligned} E_1(\boldsymbol{k}) = &\pm\{t'^2 + 2t^2 + 2tt'(\cos\boldsymbol{k}\cdot\boldsymbol{a}_1 + \cos\boldsymbol{k}\cdot\boldsymbol{a}_2) \\ &+ 2t^2\cos\boldsymbol{k}\cdot(\boldsymbol{a}_1+\boldsymbol{a}_2)\}^{1/2} + \mu_e. \end{aligned} \tag{2}$$

When $t' = t$, this gives the Dirac dispersion as in graphene, while when $t' \neq t$, a gap opens at the Dirac points. The Y point is given by $\boldsymbol{k}_\mathrm{Y} = \frac{1}{2}(\boldsymbol{b}_1 + \boldsymbol{b}_2)$ where $\boldsymbol{b}_1$ and $\boldsymbol{b}_2$ are the basic reciplocal wave vectors. Thus the eigenvalues are $E_1(\boldsymbol{k}_\mathrm{Y}) = \pm|t' - 2t| + \mu_e$ and when $t' > 2t$, the eigenvector of the upper band is

$$\frac{1}{\sqrt{2}}\begin{pmatrix}1\\-1\end{pmatrix}, \tag{3}$$

which explains the absence of the wave function amplitude on the hydrogen atom. This result is consistent with the α_3-band in Fig. 7(c). Since the p_z orbital of boron site is close to the hydrogen atoms with positive charge, the relative energy of this p_z orbital is lower than that of the σ-bonds which are away from the hydrogen atoms. This will be the reason why the p_z orbital forms an electron pocket.

The hole-like α_1-band on the Γ point consists of σ-bonds between boron atoms. Thus, we use two s-orbital-like bases on $\boldsymbol{a}_1/2$ and $\boldsymbol{a}_2/2$, as shown as blue and red circles in Fig. 8(a). The tight-binding model should be

$$\begin{aligned} H = &\, s\sum_j \left(c^\dagger_{\mathrm{D},\boldsymbol{R}_j} c_{\mathrm{D},\boldsymbol{R}_j+\boldsymbol{a}_2} + c^\dagger_{\mathrm{E},\boldsymbol{R}_j} c_{\mathrm{E},\boldsymbol{R}_j+\boldsymbol{a}_1}\right) + \mathrm{H.c.} \\ &- s'\sum_j \left(c^\dagger_{\mathrm{D},\boldsymbol{R}_j} c_{\mathrm{E},\boldsymbol{R}_j+\boldsymbol{a}_1} + c^\dagger_{\mathrm{E},\boldsymbol{R}_j} c_{\mathrm{D},\boldsymbol{R}_j+\boldsymbol{a}_2}\right) + \mathrm{H.c.} \\ &+ s''\sum_j \left(c^\dagger_{\mathrm{D},\boldsymbol{R}_j} c_{\mathrm{D},\boldsymbol{R}_j+\boldsymbol{a}_1+\boldsymbol{a}_2} + c^\dagger_{\mathrm{E},\boldsymbol{R}_j} c_{\mathrm{E},\boldsymbol{R}_j+\boldsymbol{a}_1+\boldsymbol{a}_2}\right) + \mathrm{H.c.} \\ &+ \mu_h\sum_j \left(c^\dagger_{\mathrm{D},\boldsymbol{R}_j} c_{\mathrm{D},\boldsymbol{R}_j} + c^\dagger_{\mathrm{E},\boldsymbol{R}_j} c_{\mathrm{E},\boldsymbol{R}_j}\right), \end{aligned} \tag{4}$$

where $c_{\mathrm{D},\boldsymbol{R}_j}$ and $c_{\mathrm{E},\boldsymbol{R}_j}$ ($c^\dagger_{\mathrm{D},\boldsymbol{R}_j}$ and $c^\dagger_{\mathrm{E},\boldsymbol{R}_j}$) are the annihilation (creation) operators of the bonding electron on the D sublattice and E sublattice [the blue circle and the red circle in Fig. 8(a), respectively] in the unit cell whose origin is located at $\boldsymbol{R}_j$. For y-direction hoppings, we assume the nearest- and second nearest-neighbor hoppings [s' and s'' in Fig. 8(a)]. We also assume the hoppings across the B-H-B bond [s in Fig. 8(a)]. μ_h in the last term represents the one-body energy level.

The energy dispersion is given by

$$\begin{aligned} E_2(\boldsymbol{k}) = &\, s(\cos\boldsymbol{k}\cdot\boldsymbol{a}_1 + \cos\boldsymbol{k}\cdot\boldsymbol{a}_2) + 2s''\cos\boldsymbol{k}\cdot(\boldsymbol{a}_1+\boldsymbol{a}_2) \\ &\pm\{s^2(\cos\boldsymbol{k}\cdot\boldsymbol{a}_1 - \cos\boldsymbol{k}\cdot\boldsymbol{a}_2)^2 \\ &+ 2s'^2(1+\cos\boldsymbol{k}\cdot(\boldsymbol{a}_1+\boldsymbol{a}_2))\}^{1/2} + \mu_h. \end{aligned} \tag{5}$$

The eigenvalues on Γ point are $E_2(\boldsymbol{k}_\Gamma) = 2s + 2s'' \pm 2|s'| + \mu_h$ and when $s' > 0$, the eigenvector of upper band is

$$\frac{1}{\sqrt{2}}\begin{pmatrix} 1 \\ -1 \end{pmatrix}. \tag{6}$$

This result is consistent with the α_1-band in Fig. 7(c). The parameters are estimated by using Wannier90 [47], $s = 0.921$ eV, $s' = 0.878$ eV, $s'' = 0.559$ eV, $\mu_h = -3.813$ eV.

The Fermi surface and electronic band structure gained from this tight-binding model are shown in Figs. 8(b) and 8(c). In Fig. 8(c), the band structure of tight-binding model is shown with red lines and DFT result is also shown with black lines for comparison. In Fig. 8(b), we can see the hole pocket around the Γ point (blue line) and strongly anisotropic electron pocket around the Y point (yellow line).

IV. CONCLUSION

In summary, we study the electronic states of free-standing layers of HB sheets synthesized from MgB_2 crystals by using a proton ion-exchange reaction and exfoliation. The electronic structure is semimetallic with an electron pocket at Y and a hole pocket at Γ in the 2D Brillouin zone. The electron band results from hydrogenation of the borophene layer. The tight-binding model for this electron band was derived and it is shown that this band consists of p_z-orbitals. On the other hand, the hole band from borophene remains in MgB_2. Its tight-binding model shows that the hole band consists of the σ-orbitals whose symmetry is different form the p_z-orbitals. This shows that a borophane sheet is an interesting material whose Fermi surfaces are made out of two orthogonal orbitals, and it can be a new 2D material for superconductive nanodevices. Moreover, the synthesis and understanding of free-standing boron sheets offer the potential of designing and developing new boron-based devices.

ACKNOWLEDGMENTS

This work was partially supported by the NewSUBARU Synchrotron Radiation Facility at the University of Hyogo, and a Grant-in-Aid for Specially Promoted Research (KAKENHI 18H03874) from the Japan Society for the Promotion of Science (JSPS). We appreciate Keishi Akada for experiments performed at the Synchrotron Radiation Research Organization at the University of Tokyo. Parts of the simulations were performed on the Numerical Materials Simulator supercomputer at the National Institute for Materials Science, Japan. M.O. was supported by KAKENHI 18H01162 from JSPS. I.T. was supported by KAKENHI 17H02912 from JSPS and by the Japan Society for the Promotion of Science through the Program for Leading Graduate Schools (MERIT).

[1] *Monatomic Two-Dimensional Layers: Modern Experimental Approaches for Structure, Properties, and Industrial Use*, edited by I. Matsuda (Elsevier, Amsterdam, 2018).
[2] K. S. Novoselov, A. Mishchenko, A. Carvalho, and A. H. C. Neto, Science **353**, 461 (2016).
[3] A. D. Franklin, Science **349**, 704 (2015).
[4] S. Yamazaki, Y. Hosomura, I. Matsuda, R. Hobara, T. Eguchi, Y. Hasegawa, and S. Hasegawa, Phys. Rev. Lett. **106**, 116802 (2011).
[5] B. Feng, B. Fu, S. Kasamatsu, S. Ito, P. Cheng, C.-C. Liu, S. K. Mahatha, P. Sheverdyaeva, P. Moras, M. Arita, O. Sugino, T.-C. Chiang, K. Wu, L. Chen, Y. Yao, and I. Matsuda, Nat. Commun. **8**, 1007 (2017).
[6] P. Vogt, P. DePadova, C. Quaresima, J. Avila, E. Frantzeskakis, M. C. Asensio, A. Resta, B. Ealet, and G. Le Lay, Phys. Rev. Lett. **108**, 155501 (2012).
[7] A. Fleurence, R. Friedlein, T. Ozaki, H. Kawai, Y. Wang, and Y. Yamada-Takamura, Phys. Rev. Lett. **108**, 245501 (2012).
[8] C.-L. Lin, R. Arafune, K. Kawahara, N. Tsukahara, E. Minamitani, Y. Kim, N. Takagi, and M. Kawai, Apple. Phys. Exp. **5**, 045802 (2012).
[9] Y. Fukaya, I. Mochizuki, M. Maekawa, K. Wada, T. Hyodo, I. Matsuda, and A. Kawasuso, Phys. Rev. B **88**, 205413 (2013).
[10] M. E. Davila, L. Xian, S. Cahangirov, A. Rubio, and G. LeLay, New J. Phys. **16**, 095002 (2014).
[11] C.-H. Lin, A. Huang, W. W. Pai, W.-C. Chen, T.-R. Chang, R. Yukawa, C.-M. Cheng, C.-Y. Mou, I. Matsuda, T.-C. Chiang, H.-T. Jeng, and S.-J. Tang, Phys. Rev. Materials **2**, 024003 (2018).
[12] Y. Fukaya, I. Matsuda, B. Feng I. Mochizuki, T. Hyodo, and S. Shamoto, 2D Materials **3**, 035019 (2016).
[13] F. Reis1, G. Li, L. Dudy, M. Bauernfeind, S. Glass, W. Hanke, R. Thomale, J. Schäfer, R. Claessen, Science **357**, 287 (2017).
[14] A. J. Mannix, X.-F. Zhou, B. Kiraly, J. D. Wood, D. Alducin, B. D. Myers, X. Liu, B. L. Fisher, U. Santiago, J. R. Guest, M. J. Yacaman, A. Ponce, A. R. Oganov, M. C. Hersam, and N. P. Guisinger, Science **350**, 1513 (2015).
[15] B. Feng, J. Zhang, S. Ito, M. Arita, C. Cheng, L. Chen, K. Wu, F. Komori, O. Sugino, K. Miyamoto, T. Okuda, and S. Meng, Adv. Mater. **30**, 1704025 (2018).
[16] B. Feng, O. Sugino, R.-Y. Liu, J. Zhang, R. Yukawa, M. Kawamura, T. Iimori, H. Kim, Y. Hasegawa, H. Li, L. Chen, K. Wu, H. Kumigashira, F. Komori, T.-C. Chiang, S. Meng, and I. Matsuda, Phys. Rev. Lett. **118**, 096401 (2017).
[17] B. Feng, J. Zhang, Ro-Ya Liu, T. Iimori, C. Lian, H. Li, L. Chen, K. Wu, S. Meng, F. Komori, and I. Matsuda, Phys. Rev. B **94**, 041408(R) (2016).
[18] S. Gupta, A. Kutana, and B. I. Yakobson, J. Phys. Chem. Lett. **9**, 2757 (2018).
[19] A. J. Mannix, Z. Zhang, N. P. Guisinger, B. I. Yakobson, and M. C. Hersam, Nat. Nanotechnol. **13**, 444 (2018).
[20] H. Nishino, T. Fujita, N. T. Cuong, S. Tominaka, M. Miyauchi, S. Iimura, A. Hirata, N. Umezawa, S. Okada, E. Nishibori, A. Fujino, T. Fujimori, S. Ito, J. Nakamura, H. Hosono, and T. Kondo, J. Am. Chem. Soc. **139**, 13761 (2017).
[21] M. Niibe, T. Tokushima, N. Takehira, and Y. Araki, J. Electron Spectrosc. Relat. Phenom. **220**, 118 (2017).
[22] M. Niibe, N. Takehira, and T. Tokushima, e-J. Surf. Sci. Nanotech. **16**, 122 (2018).

[23] M. Niibe, T. Kotaka, and T. Mitamura, J. Phys. Conf. Ser. **425**, 132008 (2013).
[24] M. Niibe and T. Tokushima, AIP Conf. Proc. **1741**, 030042 (2016).
[25] S. Yamamoto, Y. Senba, T. Tanaka, H. Ohashi, T. Hirono, H. Kimura, M. Fujisawa, J. Miyawaki, A. Harasawa, T. Seike, S. Takahashi, N. Nariyama, T. Matsushita, M. Takeuchi, T. Ohata, Y. Furukawa, K. Takeshita, S. Goto, Y. Harada, S. Shin, H. Kitamura, A. Kakizaki, M. Oshima, and I. Matsuda, J. Syn. Rad. **21**, 352 (2014).
[26] P. Hohenberg and W. Kohn, Phys. Rev. **136**, B864 (1964).
[27] W. Kohn and L. J. Sham, Phys. Rev. **140**, A1133 (1965).
[28] P. Giannozzi, S. Baroni, N. Bonini, M. Calandra, R. Car, C. Cavazzoni, D. Ceresoli, G. L. Chiarotti, M. Cococcioni, Ismaila Dabo, A. D. Corso, S. de Gironcoli, S. Fabris, G. Fratesi, R. Gebauer, U. Gerstmann, C. Gougoussis, A. Kokalj, M. Lazzeri, L. Martin-Samos1, N. Marzari, F. Mauri, R. Mazzarello, S. Paolini, A. Pasquarello, L. Paulatto, C. Sbraccia1, S. Scandolo, G. Sclauzero, A. P Seitsonen, A. Smogunov, P. Umari, and R. M Wentzcovitch, J. Phys.: Condens. Matter **21**, 395502 (2009).
[29] B. Ravel and M. Newville, J. Synchrotron Radiat. **12**, 537 (2005).
[30] J. Stohr, *NEXAFS Spectroscopy* (Springer, New York, 1992).
[31] N. Miyata, T. Imazono, M. Yanagihara, M. Watanabe, T. Muranaka, and J. Akimitsu, J. Phys. Soc. Jpn. **72**, 1810 (2003).
[32] E. Z. Kurmaev, I. I. Lyakhovskaya, J. Kortus, A. Moewes, N. Miyata, M. Demeter, M. Neumann, M. Yanagihara, M. Watanabe, T. Muranaka, and J. Akimitsu, Phys. Rev. B **65**, 134509 (2002).
[33] S. H. Bauer, J. Am. Chem. Soc. **59**, 1096 (1937).
[34] I. Mayer, J. Mol. Struct. **186**, 43 (1989).
[35] T. A. Abtew, B. C. Shih, P. Dev, V. H. Crespi, and P. Zhang, Phys. Rev. B **83**, 094108 (2011).
[36] Y. Jian, F. Ma, J. Bell, A. Bilic, and A. Du, Angew. Chem. Int. Ed. **55**, 10292 (2016).
[37] J. P. Perdew, K. Burke, and M. Ernzerhof, Phys. Rev. Lett. **77**, 3865 (1996).
[38] E. Bianco, S. Butler, S. Jiang, O. D. Restrepo, W. Windl, and J. E. Goldberger, ACS Nano **7**, 4414 (2013).
[39] C. Liu, I. Matsuda, R. Hobara, and S. Hasegawa, Phys. Rev. Lett. **96**, 036803 (2006).
[40] A. D. Corso, Comput. Mater. Sci. **95**, 337 (2014).
[41] E. Nishibori, M. Takata, M. Sakata, H. Tanaka, T. Muranaka, and J. Akimitsu, J. Phys. Soc. Jpn. **70**, 2252 (2001).
[42] S. Souma, Y. Machida, T. Sato, T. Takahashi, H. Matsui, S. C. Wang, H. Ding, A. Kaminski, J. C. Campuzano, S. Sasaki, and K. Kadowaki, Nature **423**, 65 (2003).
[43] S. L. Budko, G. Lapertot, C. Petrovic, C. E. Cunningham, N. Anderson, and P. C. Canfield, Phys. Rev. Lett. **86**, 1877 (2001).
[44] C. J. Bradley and A. P. Cracknell, *The Mathematical Theory of Symmetry in Solids: Representation Theory for Point Groups and Space Groups* (Oxford University Press, New York, 1972).
[45] E. S. Penev, A. Kutana, and B. I. Yakobson, Nano Lett. **16**, 2522 (2016).
[46] M. Gao, Q.-Z. Li, X.-W. Yan, and J. Wang, Phys. Rev. B **95**, 024505 (2017).
[47] A. A. Mostofi, J. R. Yates, Y.-S. Lee, I. Souza, D. Vanderbilt, and N. Marzari, Comput. Phys. Commun. **178**, 685 (2008).